Frustration of the Isotropic-Columnar Phase Transition of Colloidal Hard Platelets by a Transient Cubatic Phase

Matthieu Marechal,* Alessandro Patti,† Matthew Dennison, and Marjolein Dijkstra
Soft Condensed Matter, Debye Institute for NanoMaterials Science, Utrecht University, Princetonplein 5, 3561 RT Utrecht, The Netherlands

(Received 5 December 2011; revised manuscript received 21 February 2012; published 14 May 2012)

Using simulations and theory, we show that the cubatic phase is metastable for three model hard platelets. The locally favored structures of perpendicular particle stacks in the fluid prevent the formation of the columnar phase through geometric frustration resulting in vitrification. Also, we find a direct link between structure and dynamic heterogeneities in the cooperative rotation of particle stacks, which is crucial for the devitrification process. Finally, we show that the lifetime of the glassy cubatic phase can be tuned by surprisingly small differences in particle shape.

DOI: 10.1103/PhysRevLett.108.206101 PACS numbers: 82.60.Nh, 64.70.M−, 64.70.pv, 82.70.Dd

Nucleation is the process whereby a metastable phase transforms into a stable one via the spontaneous formation of a cluster of the stable phase. According to classical nucleation theory, the free-energy barrier that separates the metastable phase from the stable state decreases with increasing supersaturation, and for quenches in the spinodal regime, the phase transformation proceeds via spinodal decomposition and coarsening. However, at sufficiently high supersaturations the motion of the particles can slow down so dramatically that the metastable state enters a glass regime.

Vitrification hampers the phase transformation as the particles cannot rearrange diffusively to form the stable phase. However, some glasses can evolve into the stable phase despite the arrested motion. The mechanism behind this so-called ''devitrification'' process is not well understood, and neither is the origin of the glass transition and its interplay with nucleation. An intriguing scenario based on geometrical frustration has been proposed, where the local order in the liquid phase is incompatible with the long-range order of the crystal phase [1]. Hence, the formation of locally favored structures in the liquid, a concept proposed by Frank to explain dynamic arrest in glassy systems [2], prevents the crystallization. This scenario has been investigated using a two-dimensional lattice-free spin glass model, where the degree of frustration against crystallization can be tuned by an additional anisotropic potential that locally favors fivefold symmetry which is incompatible with the crystalline ground state of this model [1].

In this Letter, we investigate the interplay between nucleation, geometrical frustration, and devitrification in a simple (more realistic) three-dimensional model system of colloidal hard platelets using computer simulations. The most common model systems for colloidal platelets are hard cut spheres (HCS), which consist of the middle section of thickness L of a sphere of diameter D, and oblate hard spherocylinders (OHSC), composed of a flat cylindrical core with diameter D and height L, and a toroidal rim with tube diameter L. OHSC are more rounded than HCS [see Fig. 1(a)], and are therefore expected to better model the shape of colloidal disks, such as polymer-coated clay platelets [3] or charge-stabilized gibbsite platelets [4]. Interestingly, for $L/D = 0.2$, the phase diagram of OHSC displays an isotropic-columnar (IC) phase transition [5], whereas a very peculiar *cubatic* phase was reported in between the isotropic and the columnar phase for HCS [6]. In this phase, the particles form small stacks of almost cubelike dimensions, which tend to align perpendicular to each other. Recently, it was shown that larger system sizes tend to destabilize the cubatic phase [7,8]. However, it remains an open question whether or not the cubatic phase is thermodynamically stable for colloidal hard platelets.

Here, we show that the cubatic phase of different model hard platelets is not stable, but should be considered as a transient phase in the IC phase transformation. In addition, we show that the degree of geometric frustration can be altered via subtle changes in the particle shape: the lifetime

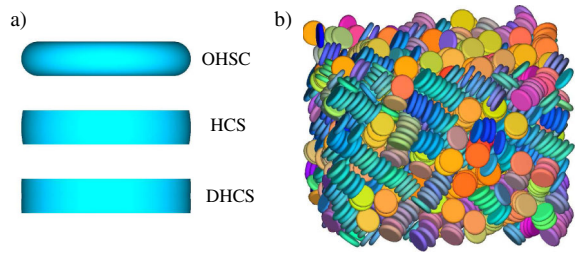

FIG. 1 (color online). (a) Three model platelets: oblate hard spherocylinders (OHSC), hard cut spheres (HCS), and double hard cut spheres (DHCS). The volumes of the particles are given by $v_{\mathrm{OHSC}} = \pi L^3/6 + \pi^2\sigma L^2/8 + \pi\sigma^2 L/4$ with $\sigma = D - L$, $v_{\mathrm{HCS}} = \pi L(3D^2 - L^2)/12$, and $v_{\mathrm{DHCS}} = \pi L[3D^2 - (L/2)^2]/12$ with L and D the (total) thickness and diameter of the particles, respectively. (b) A typical configuration of a cubatic phase of OHSC with $L/D = 0.2$ and $P^* = 11.25$ ($\eta \simeq 0.57$). Different colors denote different orientations.

of the cubatic phase increases considerably for particles with sharper edges.

We first consider a suspension of N OHSC with aspect ratio $L/D = 0.2$ in a volume V or at a pressure P. This system displays a bulk transition from an isotropic phase with packing fraction $\eta_I \equiv v_{\mathrm{OHSC}} N/V = 0.5050$ to a columnar phase with $\eta_C = 0.5691$ at pressure $P^* = \beta P v_{\mathrm{OHSC}} = 8.27$, where $\beta = 1/k_B T$ and v_{OHSC} is the volume of the OHSC particle [5].

In order to study the spontaneous formation of the columnar phase from the isotropic fluid phase, we require a cluster criterion that enables us to identify the columnar clusters. Unfortunately, the cluster criterion that was introduced to study nucleation of the nematic, smectic, and crystal phase in systems of colloidal hard rods [10–12], is not strict enough to identify columnar clusters. We therefore developed a new cluster criterion that enables us to detect hexagonal columnar clusters, which goes beyond the identification of single columns [13]. Particles are considered eligible for inclusion into a columnar cluster if they have sufficient neighbors with columnar order. Neighbors are considered to have columnar order when they have sufficient hexagonal order, as measured by a standard order parameter, but do not show high ordering with another symmetry. See Supplemental Material [14] for technical details on the cluster criterion.

We use event driven molecular dynamics (MD) simulations of relatively large system sizes ($N = 1500$, 3000, and 10 000) to study the kinetics of the IC phase transformation. Time is measured in units of $\tau_{\mathrm{MD}} = \sqrt{\beta m D^2}$, where m is the mass of an OHSC. For $\eta \geq 0.56$, we observe the immediate formation of short stacks of OHSC in the supersaturated isotropic fluid phase, which subsequently tend to orient perpendicular to each other to optimize the packing. The symmetry of these locally favored structures in the resulting cubatic phase is incompatible with that of the columnar phase, and hence the cubatic orientational order can be seen as geometric frustration against the formation of the columnar phase. The cubatic order is more pronounced for higher η and smaller system sizes ($N = 1500$ and 3000). A typical configuration of such a cubatic phase is shown in Fig. 1(b) for $\eta = 0.57$. However, in very long simulations the cubatic phase always transforms into a columnar phase. In order to analyze the phase transformation, we show the time evolution of the largest columnar cluster identified by our cluster criterion in Fig. 2(a) for $\eta = 0.56$ and 0.57. We clearly observe that the cluster grows much slower for lower η due to the lower supersaturation. In addition, we present typical configurations of postcritical columnar clusters in Figs. 2(b) and 2(d). At a packing fraction of $\eta = 0.56$, we observe one columnar cluster that grows further to form the stable columnar phase, while for $\eta = 0.57$, three postcritical clusters are observed as the nucleation barrier is much lower. Interestingly, the nematic directors of the columnar

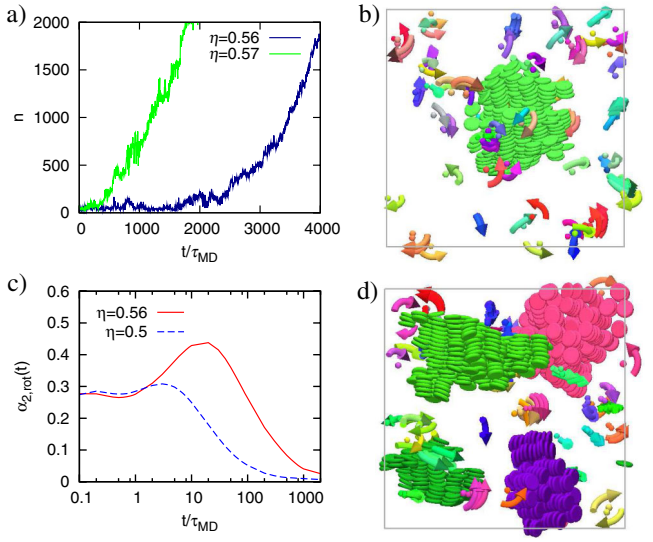

FIG. 2 (color online). (a) The size of the largest columnar cluster n in an MD simulation of an isotropic fluid of $N = 10\,000$ OHSC with $L/D = 0.2$ at packing fraction $\eta = 0.56$ and $\eta = 0.57$. (b), (d) Typical configurations of the largest columnar clusters, when the size of the largest cluster is around 300 particles (postcritical) for $\eta = 0.56$ (b) and $\eta = 0.57$ (d). Different colors of the particles denote different orientations. Swiftly rotating fluid particles are denoted by arrows pointing into the direction of the rotation; the other fluid particles are not shown at all. (c) The rotational non-Gaussian parameter [9] as a function of the time t in units of τ_{MD} (see text) for $\eta = 0.5$ and $\eta = 0.56$.

clusters are aligned along the three preferred axes of the cubatic phase, where it originated from, see Fig. 2(d). We conclude that the IC phase transformation proceeds via a transient cubatic phase and corresponds to a nucleation and growth scenario in which a spontaneously formed columnar cluster grows out to form the stable columnar phase. During MD simulations with $N = 10\,000$, we observe the appearance of columnar clusters before long-range cubatic order appeared after quick compression. In fact, this was to be expected, as the time it takes for the cubatic order to spread throughout the system increases with system size, while the time for a nucleus to form in a fixed volume is system size independent. Therefore, the behavior observed in experiments, such as the Cryo-TEM experiments in which the cubatic phase was observed [3], is largely dependent on the sample volume, which for Cryo-TEM is rather small to allow sufficiently fast shock-freezing of the sample. This suggests that the cubatic phase may be stabilized by confinement.

Additionally, we investigated the translational and orientational dynamics of the particles in the supersaturated fluid of OHSC. To this end, we calculate the mean square translational displacement $\langle |\mathbf{r}_i(t) - \mathbf{r}_i(0)|^2 \rangle$ and the mean square rotational displacement $\langle |\Delta \boldsymbol{\varphi}_i(t)|^2 \rangle$ (not shown), where the angular brackets indicate an ensemble average, $\mathbf{r}_i(t)$ and $\Delta \boldsymbol{\varphi}_i(t) = \int_0^t \boldsymbol{\omega}_i(t) dt$ are the position and the

angular displacement [9], respectively, of particle i at time t with $\boldsymbol{\omega}$ the angular velocity. The corresponding translational and rotational diffusion constants measured in event-driven MD simulations [14] show a clear slowing down of the translational and rotational dynamics by about a factor of $\simeq 5$ when the packing fraction is increased from $\eta = 0.5$ to 0.56. The simultaneous slowing down of the translational and rotational dynamics should be contrasted with the decoupling of the freezing of the translational and rotational degrees of freedom that is found for hard ellipsoids [15,16], as well for the attractive-repulsive Gay-Berne ellipsoids [17,18]. We expect that the translational and rotational dynamics are strongly coupled in all systems that form stacks or columns in the isotropic fluid. This very likely includes those experimental discotic systems that display direct IC phase transition. The rotational dynamics of such a system is investigated in Ref. [19].

Heterogeneous dynamics in the form of collective particle reorientations is found in the locally cubatic fluid, as can be appreciated from Figs. 2(b) and 2(d), where we represent all fluid particles that rotate swiftly by arrows denoting the direction of the rotation. Quantitative evidence for heterogeneous dynamics is given in Fig. 2(c), where the rotational non-Gaussian parameter [9] defined as $\alpha_{2,\mathrm{rot}}(t) \equiv 3\langle|\Delta\boldsymbol{\varphi}_i(t)^4\rangle/5\langle|\Delta\boldsymbol{\varphi}_i(t)|^2\rangle^2 - 1$ is shown. The pronounced increase in the peak height of $\alpha_{2,\mathrm{rot}}(t)$ when the density is increased from $\eta = 0.5$ to $\eta = 0.56$ is a clear sign of the emergence of heterogeneous dynamics [9]. We wish to remark here that the simultaneously rotating clusters can be easily identified here as small stacks of up to four particles, which is impossible for glassy states of spherical particles where heterogeneous dynamics cannot be easily related to the local structure [21]. Similarly, the growth of a columnar phase often proceeds by collective attachment of small stacks rather than single particles [14]. Interestingly, the rotation of stacks also plays a crucial role in the late-stage development of the columnar cluster. Figure 3 shows a form of defect healing in which a stack of misaligned particles in the columnar cluster first breaks up into smaller stacks and, subsequently, these smaller stacks reorient to conform with the director of the cluster.

As nucleation of a columnar phase from a glassy state with cubatic order is hardly studied, it is interesting to determine the nucleation barrier associated for this devitrification process. Since the equilibration can only proceed via collective rearrangement of small clusters, the formation of the columnar phase is severely hampered by slow dynamics. We determine the nucleation barrier by employing the umbrella sampling technique in Monte Carlo (MC) simulations [10]. The resulting Gibbs free energy barrier $\Delta G(n)$ as a function of columnar cluster size n for OHSC with $L/D = 0.2$ and $\eta = 0.550$ and 0.569 is shown in Fig. 4. As equilibration is rather slow due to glassy dynamics, the noise on $\Delta G(n)$ is significant. However, we are able to determine for the first time a nucleation barrier for a

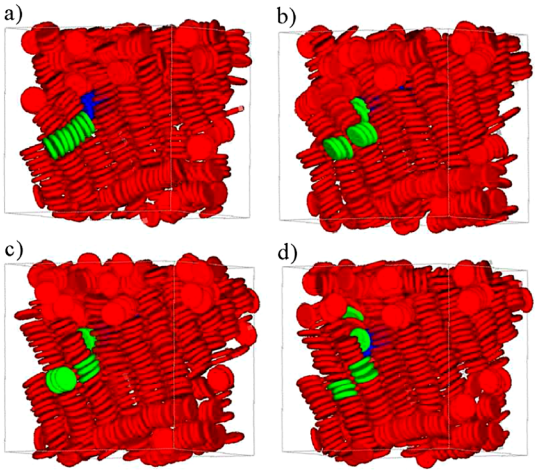

FIG. 3 (color online). (a) A long stack of (green) particles, which is oriented perpendicular to the nematic director of the columnar phase, is divided in smaller packages of two to four particles as shown in (b). Subsequently, these smaller packages of particles can rotate by 90 deg as shown in (c) and (d) in such a way that the orientation matches the columnar phase.

devitrification process in which a glassy state transforms into a stable phase via collective particle reorientations. We also present typical configurations of the critical nucleus that corresponds with the top of the barrier in Fig. 4 along with the critical nucleus obtained from MD simulations at $\eta = 0.56$. We find that the results for the structure and shape of the critical nucleus as obtained from MC or MD simulations are very similar; i.e., the cluster consists of an hexagonal array of particle stacks and the overall shape of the cluster is roughly spherical. The barrier height is $\beta\Delta G^*(n) \simeq 15$ and 12 for $\eta = 0.550$ and 0.569, respectively. We mention here that the corresponding values for

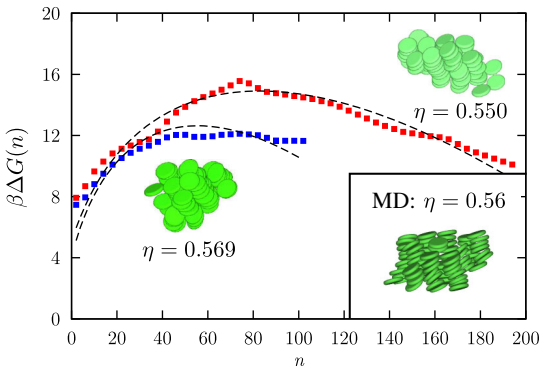

FIG. 4 (color online). Gibbs free energy $\beta\Delta G(n)$ as a function of the number of particles n in the largest columnar cluster for a system of OHSC with $L/D = 0.2$ and packing fraction $\eta = 0.550$ and 0.569 (squares). The dashed line is a fit [22] to classical nucleation theory. Configurations of the critical nucleus are shown obtained from MC simulations for $\eta = 0.550$ and 0.569 in the main panel and from MD simulations at $\eta = 0.56$ in the inset.

the supersaturation $\beta\Delta\mu = 0.414$ and 0.553, which is the driving force for nucleation, is extremely small; for comparison we note that, for hard spheres at $\eta = 0.5478$, $\beta\Delta\mu \simeq 0.74$, which leads to fast nucleation [22].

Our results show clearly that the cubatic phase of OHSC is metastable with respect to an IC phase transition. In this light, it is interesting to study the effect of particle shape on the stability of the cubatic phase. To this end, we measure the cubatic order parameter [7] as a function of pressure for the three particle shapes depicted in Fig. 1 using NPT MC simulations with $N = 3000$ particles. The shapes (ordered from more curved to more cylinderlike) are OHSC, HCS, which resemble recently synthesized particles of Ref. [24], and double hard cut spheres (DHCS). The latter model consists of two superimposed HCS and is essentially a cylinder. All three models have the same height-to-diameter ratio of $L/D = 0.2$. The onset of cubatic order, as defined by the packing fraction η_{cub} at which the cubatic order parameter suddenly increases, is shown as the dashed, blue line in Fig. 5. We observe clearly that η_{cub} decreases upon decreasing the particle curvature. Furthermore, η_{cub} for $N = 3000$ HCS is essentially equal to that of the largest system size, $N = 1728$, of Ref. [7], indicating that finite size effects beyond $N = 3000$ are small.

In addition, we study the stability of the cubatic phase using a high-order virial theory. In Ref. [7], it was shown that an eighth order expansion is required to predict a stable isotropic-cubatic phase transition for HCS with $L/D = 0.2$. Here, we apply this theory to predict the isotropic-cubatic phase transition for OHSC, HCS (with higher precision than in Ref. [7]), and DHCS. The results for the bulk density of the cubatic phase in coexistence with the isotropic phase are denoted by the dashed, red lines in Fig. 5(c) at the eighth virial level. Although, the agreement with the simulations results is not satisfactory, surprisingly, the trend of the bulk density of the cubatic phase with particle curvature is very similar to that of the NPT MC simulations.

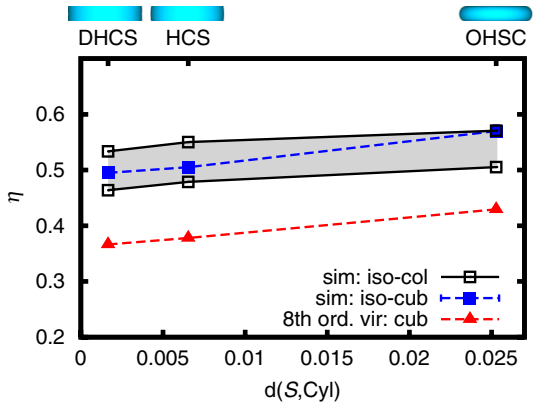

FIG. 5 (color online). The phase diagram for double hard cut spheres (DHCS), hard cut spheres (HCS) and OHSC with $L/D = 0.2$: packing fraction η versus $d(S, \mathrm{Cyl})$, the difference [14,23] between the shape S in question and a cylinder (Cyl) with the same volume and aspect ratio. The gray area and the black lines denote coexistence between the isotropic and the columnar phase from simulations [14]. The metastable transition from the isotropic to the cubatic phase is denoted by the dashed lines, where the solid squares denote simulation results for $N = 3000$ particles, and the triangles denote the results from an eighth order virial theory.

Finally, we determine the stability of the cubatic phase with respect to the columnar phase for HCS and DHCS. The apparent stability of the cubatic phase for HCS could be due to dynamic arrest. Inspired by the particle stack rotations as observed in our MD simulations, we introduce a new cluster move in the MC simulations to speed up equilibration [14]. In order to investigate more precisely the location of the phase coexistence between the isotropic or cubatic fluid phase with the columnar phase, we perform NPT MC simulations of the two coexisting phases in a simulation box that is large enough that the interfacial free energy is sufficiently small [25,26]. The coexistence pressure can be determined as the pressure at which neither of the phases grows at the expense of the other phase [14,26]. The corresponding coexistence densities for HCS and DHCS are shown in Fig. 5. Clearly, the pressure at which the columnar phase becomes more stable than the isotropic phase is lower than the pressure at which long-range cubatic order was found, which unambiguously shows that the cubatic phase is unstable for all three shapes considered. The strong decrease of η_{cub} as the particle shape changes from OHSC to HCS causes a strong decrease in $\Delta\mu$ and, therefore, a strong increase in the lifetime of the cubatic phase, see also Fig. S4 [14].

In conclusion, we find that the cubatic phase is metastable with respect to an IC phase coexistence for all three model platelets, and can be regarded as a transient phase in the IC phase transformation. The locally favored structures of perpendicularly oriented particle stacks in the cubatic phase leads to geometric frustration that prevents the formation of the columnar phase thereby yielding vitrification. Additionally, we find a direct link between structural order and dynamic heterogeneities provided by the cooperative rotation of particle stacks in the cubatic phase. Such a link is often assumed to be characteristic for glassy behavior, but is not easy to demonstrate in e.g., colloidal hard sphere glasses. We also show that the cooperative stack rotations play an important role in the devitrification process and that the lifetime of the cubatic phase can be tuned by confinement and by surprisingly small differences in the particle shape. Interestingly, our results explain recent experimental observations on suspensions of gibbsite platelets which enter a kinetically arrested glass regime upon increasing the particle concentration and in which small iridescent grains of the columnar phase were formed after periods of months to years [4].

*Present address: Heinrich Heine University, Düsseldorf, Germany.

†Present address: Institute of Advanced Chemistry of Catalonia-CSIC, C/Jordi Girona 18-26, 08034, Barcelona, Spain.

[1] H. Shintani and H. Tanaka, Nature Phys. **2**, 200 (2006).
[2] F. C. Frank, Proc. R. Soc. A **215**, 43 (1952).
[3] S. J. S. Qazi, G. Karlsson, and A. R. Rennie, J. Colloid Interface Sci. **348**, 80 (2010).
[4] M. C. D. Mourad, A. A. Verhoeff, D. V. Byelov, A. V. Petukhov, and H. N. W. Lekkerkerker, J. Phys. Condens. Matter **21**, 474218 (2009).
[5] M. Marechal, A. Cuetos, B. Martínez-Haya, and M. Dijkstra, J. Chem. Phys. **134**, 094501 (2011).
[6] J. A. C. Veerman and D. Frenkel, Phys. Rev. A **45**, 5632 (1992).
[7] P. D. Duncan, M. Dennison, A. J. Masters, and M. R. Wilson, Phys. Rev. E **79**, 031702 (2009).
[8] P. D. Duncan, A. J. Masters, and M. R. Wilson, Phys. Rev. E **84**, 011702 (2011).
[9] M. G. Mazza, N. Giovambattista, F. W. Starr, and H. E. Stanley, Phys. Rev. Lett. **96**, 057803 (2006).
[10] A. Cuetos and M. Dijkstra, Phys. Rev. Lett. **98**, 095701 (2007).
[11] A. Patti and M. Dijkstra, Phys. Rev. Lett. **102**, 128301 (2009).
[12] R. Ni, S. Belli, R. van Roij, and M. Dijkstra, Phys. Rev. Lett. **105**, 088302 (2010).
[13] R. Berardi, M. Cecchini, and C. Zannoni, J. Chem. Phys. **119**, 9933 (2003).
[14] See Supplemental Material at http://link.aps.org/supplemental/10.1103/PhysRevLett.108.206101 for movies and technical details.
[15] C. De Michele, R. Schilling, and F. Sciortino, Phys. Rev. Lett. **98**, 265702 (2007).
[16] M. Letz, R. Schilling, and A. Latz, Phys. Rev. E **62**, 5173 (2000).
[17] D. Chakrabarti, P. P. Jose, S. Chakrabarty, and B. Bagchi, Phys. Rev. Lett. **95**, 197801 (2005).
[18] D. Chakrabarti and B. Bagchi, Phys. Rev. Lett. **96**, 187801 (2006).
[19] J. Li, K. Fruchey, and M. D. Fayer, J. Chem. Phys. **125**, 194901 (2006).
[20] The particles do not rotate around their symmetry axis in our EDMD. Therefore, the diffusion at short times seems two-dimensional, while our definition of $\alpha_2(t)$ is for three dimensions. As a result, $\lim_{t\to 0}\alpha_2(t)$ is larger than zero.
[21] E. Sanz, C. Valeriani, E. Zaccarelli, W. C. K. Poon, P. N. Pusey, and M. E. Cates, Phys. Rev. Lett. **106**, 215701 (2011).
[22] L. Filion, M. Hermes, R. Ni, and M. Dijkstra, J. Chem. Phys. **133**, 244115 (2010).
[23] M. Moszyńska, *Selected Topics in Convex Geometry* (Birkhäuser, Boston, 2006).
[24] T. Fujibayashi and M. Okubo, Langmuir **23**, 7958 (2007).
[25] C. Vega, E. P. A. Paras, and P. A. Monson, J. Chem. Phys. **96**, 9060 (1992).
[26] T. Zykova-Timan, J. Horbach, and K. Binder, J. Chem. Phys. **133**, 014705 (2010).

Frustration of the isotropic-columnar phase transition of colloidal hard platelets by a transient cubatic phase: Supplementary Material

Matthieu Marechal,* Alessandro Patti,† Matthew Dennison, and Marjolein Dijkstra

Soft Condensed Matter, Debye Institute for NanoMaterials Science, Utrecht University, Princetonplein 5, 3561 RT Utrecht, The Netherlands

(Dated: February 20, 2012)

Cluster criterion

The cluster criterion consists of the following steps: First, we define the neighbors of particle i as those particles j for which the surface-to-surface distance ρ_{ij} is smaller than $0.2D$ and $\mathbf{u}_i \cdot \mathbf{u}_j > 0.9$ with $\mathbf{u}_i$ the orientation of particle i. We also define the set of particles $\mathcal{E}_i$ which contains i and its neighbors and we define the plane $\mathcal{P}_i$ perpendicular to the nematic director $\mathbf{n}_i$ of the particles in $\mathcal{E}_i$. Then, we examine the trigonal, square and hexagonal order around particle i in the plane $\mathcal{P}_i$,

$$\psi_n(i) = \left| \frac{1}{N_b(i)} \sum_{j=1}^{N_b(i)} \exp(\,\mathrm{i}\, n\phi_{ij}) \right|, \tag{1}$$

where $n = 3, 4, 6$, and ϕ_{ij} is the angle between $\mathbf{r}_{ij}^{\mathrm{proj}}$ and a reference axis, which lies in $\mathcal{P}_i$. Also, $\mathbf{r}_{ij}^{\mathrm{proj}}$ is the projection on $\mathcal{P}_i$ of the bond between particle i and j. The sum over j runs over the $N_b(i)$ neighbors of particle i which are not in the same stack as i (the values for ϕ_{ij} for j in the same stack as i are random for both isotropic and columnar phases). Furthermore, particles i and j are defined to be in the same stack if they are neighbors and their center-to-center distance r_{ij} is smaller than $L + 0.2D$. We then make a distinction between particles with a columnar-like and an isotropic-like environment. Particle i has a columnar-like environment if $\psi_6(i) > 0.6$ and $\psi_n(i) < 0.7$ for $n = 3, 4$. We define $n_{\mathrm{col}}(i)$ to be the number of particles in $\mathcal{E}_i$ that have a columnar-like environment. Those particles i that have $n_{\mathrm{col}}(i) \geq 4$ are called columnar particles. Finally, two columnar particles are part of the same cluster, if they are neighbors.

Stack rotation moves

To speed up the equilibration of Monte Carlo simulations, especially the ones with hard cut spheres and double hard cut spheres, we implemented Monte Carlo moves that are designed specifically to rotate short stacks. We select a particle randomly and define a stack by the particles with a center-to-center distance smaller than the $0.5D$. The nematic axis of this stack is determined in the usual way [1] and a random vector in the plane perpendicular to this axis is generated. The stack is rotated around this axis by ninety degrees. Finally, the move is accepted if no overlaps are generated and rejected otherwise. This move can easily be seen to obey detailed balance. Furthermore, the simulation is ergodic because regular rotation and translation moves are also performed. Although the acceptance ratio of these moves is tiny 10^{-6}, the small number of moves that are accepted during the simulation do significantly speed up the simulation.

Coexistence

We simulate two coexisting phases, a columnar phase and an isotropic or cubatic phase, in a single, rectangular simulation box. The initial configurations of these NPT MC simulations consist of two phases of interest in contact. The simulation box has to be sufficiently long in the direction perpendicular to the interface, such that the effect of the interface on either of the coexisting phases is small. While this dimension fluctuates in the simulation, the other dimensions are kept fixed at the values obtained in a prior NPT MC

* Currently at HHU, Düsseldorf, Germany
† Currently at IQAC-CSIC, Barcelona, Spain

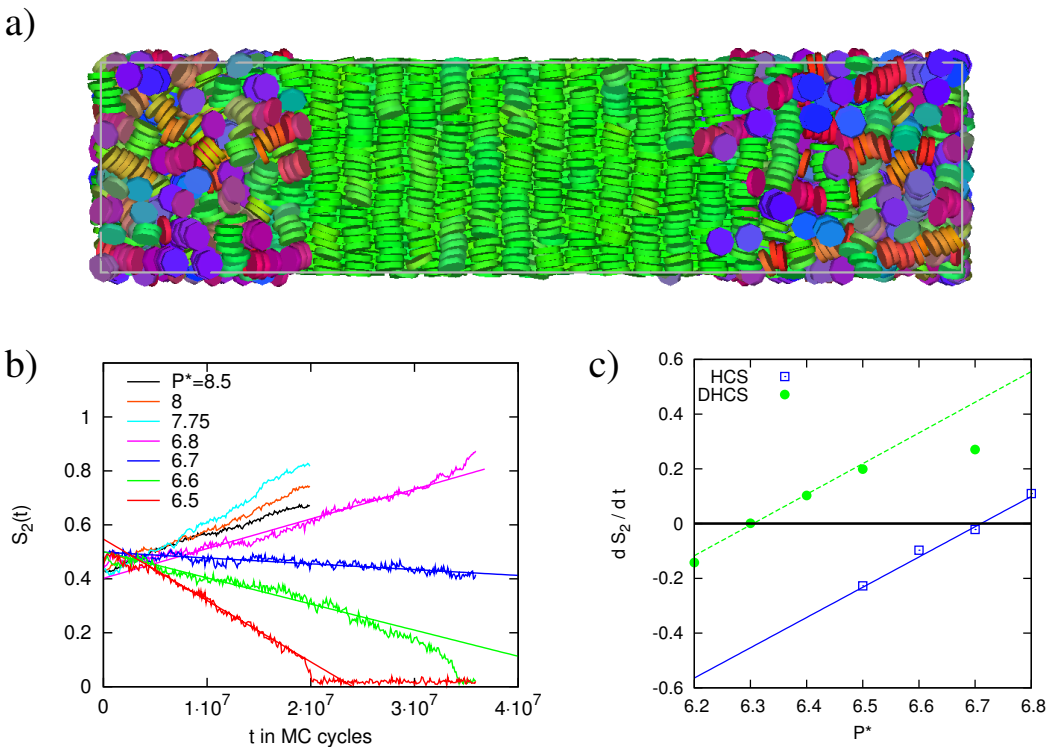

FIG. S1. (a) The initial configuration of each of the simulations in which we determine the pressure at coexistence between the isotropic phase and the columnar phase consists of a fluid phase and a columnar phase joined together in a single simulation box for cut spheres after equilibration at $P^* = 6.8$. (b) Nematic order parameter S_2 versus the number of MC cycles in NPT simulations of cut spheres at pressures $P^* \equiv \beta P v_{\rm CS}$ as labeled. The straight lines are linear fits to the straigth sections of the curves. (c) The fits from (b) as a function of the pressure P^* and the corresponding plot for double hard cut spheres. The straight lines are linear fits. The outlier for DHCS is too far from coexistence to fall on a straight line (see text) and is therefore not included in the fit.

simulation of only the bulk positionally ordered phase (the columnar phase). In the latter simulation, all three dimensions were allowed to adapt to a change in pressure. A typical snapshot of a simulation after initial equilibration, during which the cubatic phase transforms into an isotropic fluid, is shown in Fig. S1(a). In Fig. S1(b), the nematic order parameters as obtained from such simulations for cut spheres and a range of pressures are shown. Clearly the cubatic phase transforms into the columnar phase for the pressures where the fluid showed system-spanning cubatic order *i.e.* for $P^* \equiv \beta P v_{HCS} \geq 7.75$. This shows unambiguously that the cubatic phase is not stable for any of the investigated densities.

Fits to the nematic order parameter [straight lines in Fig. S1(b)] near the coexistence can be used to determine the coexistence pressure [3]. This process is shown in Fig. S1(c). The slope of the linear fits to $S_2(t)$ is denoted $d\,S_2(t)\,/\,d\,t$. The coexistence pressure is the pressure for which $d\,S_2(t)\,/\,d\,t = 0$. The growth speed can be shown to be proportional to $D[\exp(\beta\Delta\mu) - 1]$ [4], where $\Delta\mu$ is the supersaturation (the chemical-potential difference between the two phases in contact) and D is the self-diffusion constant. Near coexistence we use this to approximate $d\,S_2(t)\,/\,d\,t \simeq a\Delta\mu = a\int(1/\rho_I - 1/\rho_C)dP \simeq b\Delta P$, where ρ_I and ρ_C are the densities of the isotropic and columnar phases, respectively. Furthermore, we assume that

Shape S	$d(S,\mathrm{Cyl})$	P^*	η_I	η_C	$\eta_{\rm cub}$
DHCS	0.00165836	6.304(7)	0.4639(4)	0.5336(3)	0.495(5)
HCS	0.00653491	6.710(8)	0.4788(4)	0.5502(3)	0.505(5)
OHSC [2]	0.02527792	8.276	0.5052	0.5705	0.57(1)

TABLE I. The pressures and packing fractions at coexistence between the isotropic (I) and columnar (C) phases for HCS and DHCS from this work and for OHSC from Ref. [2]. Also shown is the Haussdorf distance $d(S,\mathrm{Cyl})$ between a cylinder (Cyl) and each of the three shapes S. Furthermore, the packing fraction $\eta_{\rm cub}$ at which the cubatic order increases suddenly on increase of the density is listed in the last column.

the pressure difference ΔP is small enough that all properties of the two phases in the simulation box are approximately equal to those of the system at coexistence, such that a and b are approximately constant. In practice, we fit a linear function to $d\,S_2(t)\,/\,d\,t$ as a function of P^* and calculate the pressure for which this straight line intersects with the line $d\,S_2(t)\,/\,d\,t = 0$ (the thick black line in Fig. S1). In Fig. S1(c), a point far from the coexistence is plotted to show that deviations from linearity are indeed a real possibility. This outlier is not included in the fit. The resulting coexistence data are listed in Tbl. I together with the data for the OHSC for reference.

Difference between shapes

The difference between shapes as plotted in the phase diagram, Fig. 5 of the main text, is defined using the Hausdorff distance [5]. In order to define this distance on shape space, which is commonly used in (convex) geometry, we first define

$$d'(A,B) = \max_{\mathbf{x}\in A}\min_{\mathbf{y}\in B}|\mathbf{x}-\mathbf{y}| \tag{2}$$

where A and B are solid (compact) bodies. The Hausdorff distance is then defined by

$$d(A,B) = \max\{d'(A,B), d'(B,A)\}. \tag{3}$$

For solid (compact) bodies, it can easily be seen that, for the two points $\mathbf{x}$ and $\mathbf{y}$ at a local minimum–maximum in Eqn. (2), (i) $\mathbf{x}$ lies on the surface ∂A of body A, while (ii) $\mathbf{y}$ lies on ∂B, (iii) $\mathbf{x}-\mathbf{y}$ is an outward normal to the surface of A in $\mathbf{x}$ and (iv) $\mathbf{x}-\mathbf{y}$ is also an outward normal to the surface of B in $\mathbf{y}$ (in the case of a cusp at one of the two points, $\mathbf{x}-\mathbf{y}$ has only to be normal to the path of the cusp at the point in question and point away from the body in question). Maximizing over all such pairs (of which there are only a few, if one takes into account the rotational symmetry) we can easily calculate the Hausdorff distance between a cylinder and an oblate hard spherocylinder, a hard cut sphere or a hard double cut sphere where all the shapes have the same aspect-ratio, volume and center-of-mass position and are co-aligned. The resulting values for the Hausdorff norm are listed in Tbl. I.

Slow and collective dynamics

In Fig. S2(a), the translational and rotational diffusion constants divided by to the respective values at $\eta = 0.5$ (near coexistence). The translational diffusion constant is defined as $\lim_{t\to\infty}\langle|\mathbf{r}_i(t)-\mathbf{r}_i(0)|^2\rangle/6t$ and the rotational diffusion constant by $\lim_{t\to\infty}\langle|\Delta\boldsymbol{\varphi}_i(t)|^2\rangle/6t$, where $\mathbf{r}_i(t)$ is the position of particle i at time t and $\Delta\boldsymbol{\varphi}_i(t)$ its angular displacement since time $t = 0$.

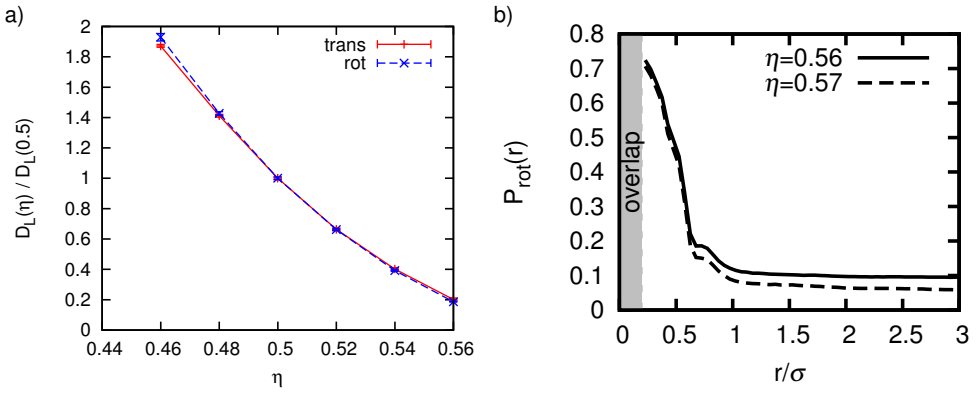

FIG. S2. (a) The rotational and translational long time diffusion constants as a function of η relative to the value at $\eta = 0.5$. For most of the density range the plots are nearl superimposed. (b) The chance $P_{\rm rot}(r) = g_{\rm rot,rot}(r)/g_{\rm rot,all}(r)$, where $g_{s,s'}(r)$ is the radial distribution function that measures the distribution of particles of type s' around particles of type s, and "all" denotes all particles, while "rot" denotes those particles that rotated more than 45 degrees between two snapshots that were taken at time intervals of $5\tau_{\rm MD}$.

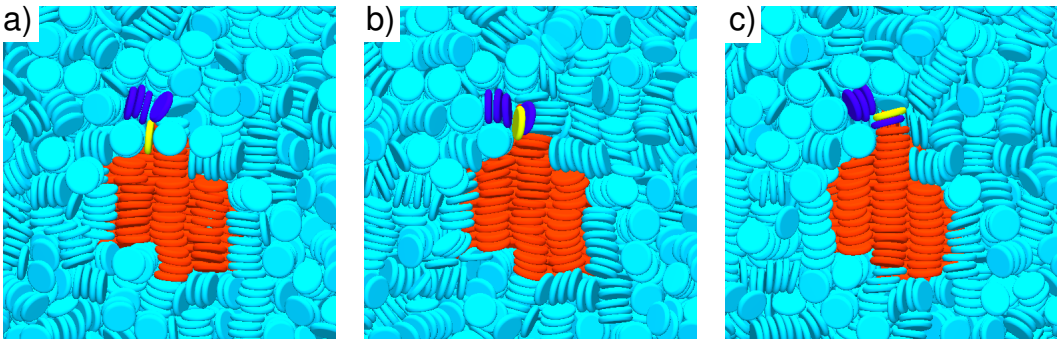

FIG. S3. (a) A particle (yellow) is misaligned with the columnar cluster (indicated by the red particles). (b) It slips in between the particles of a stack (dark blue). (c) Together with one of the particles of the stack, it rotates and becomes part of the columnar cluster.

The main mode of re-orientation is the collective rotation of the particle in a stack as can be seen in Fig. S2(c), which shows that, when a particle rotates more than 45 degrees, more than 60% of its neighbors with a center-of-mass distance smaller than $2L$ rotate along. This has consequences for the attachment to the columnar cluster, as shown in Fig. S3.

Life time of the cubatic phase

According to classical nucleation theory, the supersaturation $\Delta\mu \equiv \mu_{\rm fluid} - \mu_{\rm col}$ drives the nucleation of the columnar phase, where $\mu_{\rm fluid}$ is the chemical potential of the isotropic/cubatic branch and $\mu_{\rm col}$ the chemical potential of the columnar phase. As cubatic order is found at a much higher packing fraction for OHSC than for HSC and DHCS and the packing fraction at the IC transition only increases weakly, the supersaturation at this packing fraction $\eta_{\rm cub}$ where the cubatic order is first found is much higher for OHSC than for HCS. However, the dynamics is also much slower. Nevertheless, the cubatic phase of OHSC transforms much faster into the columnar phase for a packing fraction just above $\eta_{\rm cub}$ for OHSC, than the cubatic phase for HCS at a packing fraction even a bit higher above $\eta_{\rm cub}$ than the OHCS system, as shown in Fig. S4. For lower densities, the system of HCS never spontaneously transformed to the columnar phase in the time window accessible in our simulations.

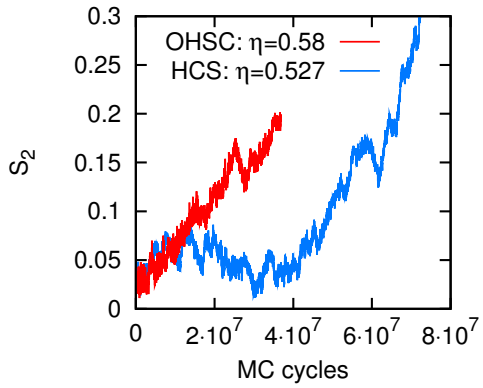

FIG. S4. The nematic order parameter S_2 for two systems as a function of the number of Monte Carlo cycles. The first system contains OHSC at $\eta = 0.58$, 2% above the isotropic–cubatic transition $\eta_{\rm cub}$, and the second HCS at $\eta = 0.58$, 4% above $\eta_{\rm cub}$.

[1] M. P. Allen, G. T. Evans, D. Frenkel, and B. M. Mulder, Advances in chemical physics **86**, 1 (1993).

[2] M. Marechal, A. Cuetos, B. Martínez-Haya, and M. Dijkstra, J. Chem. Phys. **134**, 094501 (2011).
[3] T. Zykova-Timan, J. Horbach, and K. Binder, J. Chem. Phys. **133**, 014705 (2010).
[4] S. Pronk and D. Frenkel, J. Chem. Phys. **110**, 4589 (1999).
[5] M. Moszyńska, *Selected topics in convex geometry* (Birkhäuser, Boston, 2006).